

Solar origin of heliospheric magnetic field inversions: Evidence for coronal loop opening within pseudostreamers

M. J. Owens,¹ N. U. Crooker,² and M. Lockwood¹

Received 19 September 2012; revised 12 March 2013; accepted 4 January 2013; published 28 May 2013.

[1] The orientation of the heliospheric magnetic field (HMF) in near-Earth space is generally a good indicator of the polarity of HMF foot points at the photosphere. There are times, however, when the HMF folds back on itself (is inverted), as indicated by suprathermal electrons locally moving sunward, even though they must ultimately be carrying the heat flux away from the Sun. Analysis of the near-Earth solar wind during the period 1998–2011 reveals that inverted HMF is present approximately 5.5% of the time and is generally associated with slow, dense solar wind and relatively weak HMF intensity. Inverted HMF is mapped to the coronal source surface, where a new method is used to estimate coronal structure from the potential-field source-surface model. We find a strong association with bipolar streamers containing the heliospheric current sheet, as expected, but also with unipolar or pseudostreamers, which contain no current sheet. Because large-scale inverted HMF is a widely accepted signature of interchange reconnection at the Sun, this finding provides strong evidence for models of the slow solar wind which involve coronal loop opening by reconnection within pseudostreamer belts as well as the bipolar streamer belt. Occurrence rates of bipolar- and pseudostreamers suggest that they are equally likely to result in inverted HMF and, therefore, presumably undergo interchange reconnection at approximately the same rate. Given the different magnetic topologies involved, this suggests the rate of reconnection is set externally, possibly by the differential rotation rate which governs the circulation of open solar flux.

Citation: Owens, M. J., N. U. Crooker, and M. Lockwood (2013), Solar origin of heliospheric magnetic field inversions: Evidence for coronal loop opening within pseudostreamers, *J. Geophys. Res. Space Physics*, 118, 1868–1879, doi:10.1002/jgra.50259.

1. Introduction

[2] On average, the large-scale heliospheric magnetic field (HMF) is generally well described by the Parker spiral. The angle of the HMF to the inward radial direction [the X axis in the Geocentric Solar Ecliptic (GSE) reference frame], ϕ_p , depends on solar wind speed, heliocentric distance, and latitude, but in near-Earth space, it is nominally centered around $135^\circ/315^\circ$ for outward/inward polarity HMF [e.g., Borovsky, 2010]. The heliospheric current sheet (HCS) separates sectors of inward and outward magnetic flux and projects back to a coronal source-surface as a neutral line marking the heliomagnetic equator. Crossings of the near-Earth HCS can be identified by rapid changes in the HMF direction from 135° to 315° , or vice versa. This is shown schematically in Figure 1a.

[3] HMF connectivity to the Sun can usually be inferred by suprathermal electron (STE) observations. Open HMF, which has one end connected to the Sun, exhibits an adiabatically focused STE beam, or “strahl,” that originates in the solar corona [Feldman *et al.*, 1975; Rosenbauer *et al.*, 1977]. Thus, outward (inward) magnetic sectors should contain a strahl which is parallel (antiparallel) to the HMF, as shown in Figure 1a. Times of counterstreaming electrons (CSEs), when both parallel and antiparallel strahls are present, reveal “closed” HMF, with both ends of the field line connected to the Sun (times 2 and 3 in Figure 1b). They are strongly associated with interplanetary coronal mass ejections [Gosling *et al.*, 1987; Wimmer-Schweingruber *et al.*, 2006], which in turn are frequently encountered at magnetic sector boundaries (Figure 1b) [Crooker *et al.*, 1998]. It should be noted that CSEs can also result on open HMF via reflection at Earth’s bow shock [e.g., Haggerty *et al.*, 2000] or interplanetary shocks [Gosling *et al.*, 1993; Steinberg *et al.*, 2005].

[4] There also exist periods with a single strahl in the opposite sense to that expected from the magnetic field direction [Kahler and Lin, 1994, 1995; Kahler *et al.*, 1996; Crooker *et al.*, 1996; Crooker *et al.*, 2004b], as shown in Figures 1c–1e. These intervals imply that the magnetic field is folded back upon itself or inverted. Inverted HMF intervals can be bounded by a change in the magnetic field

¹Space Environment Physics Group, Department of Meteorology, University of Reading, Reading, Berkshire, UK.

²Center for Space Physics, Boston University, Boston, Massachusetts, USA.

Corresponding author: M. J. Owens, Space Environment Physics Group, Department of Meteorology, University of Reading, Earley Gate, PO Box 243, Reading, Berkshire RG6 6BB, UK. (m.j.owens@reading.ac.uk)

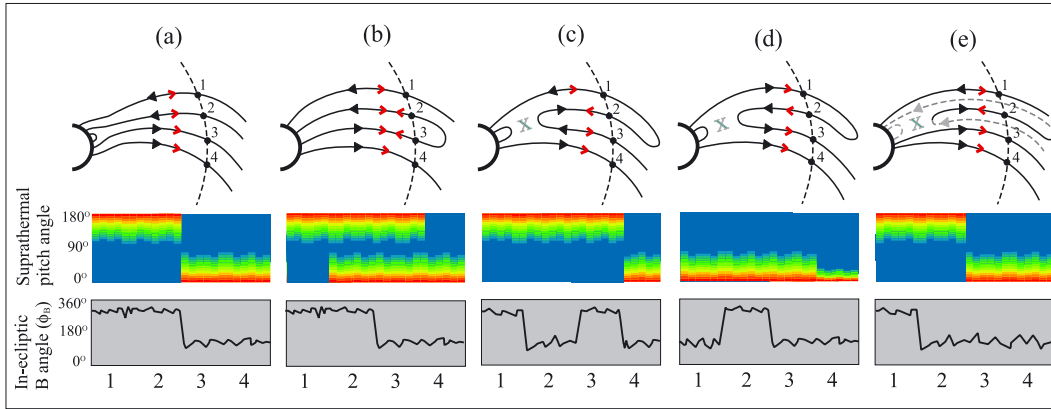


Figure 1. Sketches of possible HMF configurations and the resulting magnetic field and suprathermal electron signatures in near-Earth space. Red (black) arrows show the thermal electron strahl (magnetic field polarity), while gray crosses show the position of magnetic reconnection. (a) A typical sector boundary/HCS crossing. (b) A sector boundary accompanied by closed HMF loops, likely part of an interplanetary coronal mass ejection (ICME). (c) A sector boundary/HCS crossing containing an inverted HMF interval at time 2. (d) An inverted HMF interval at time 2 embedded within a unipolar region. (e) A sector boundary with mismatched electron and magnetic signatures. The dashed lines show portions of the inverted HMF structure which are out of the ecliptic plane and not encountered by the observing spacecraft [after Crooker *et al.*, 2004b].

direction with no change in the strahl direction and vice versa. Pairs of the former are common and can be found both near the HCS, as in Figure 1c, and in unipolar regions [e.g., Balogh *et al.*, 1999], as in Figure 1d (Note that while the strahl direction will not change, the strength or width of the strahl could change with changing solar connectivity.) These pairs of field changes bound inversions that are usually of short duration, on the order of an hour or two. In contrast, inversions bounded on at least one side by a change in the strahl direction with no change in the magnetic field direction are less common but can be of long duration, on the order of a day or more [Crooker *et al.*, 2004b]. Moreover, they can only be understood in terms of a three-dimensional structure. In cases involving the HCS, as in Figure 1e, where the dashed field lines lie out of the plane of the figure, the inversion results in a mismatch between the magnetic and electron signatures of the sector boundary [Crooker *et al.*, 2004b].

[5] While some of the smaller inversions may be the product of large-scale turbulent processes, the larger inversions appear to be robust signatures of near-Sun magnetic interchange reconnection, as sketched in Figures 1c–1e, where a green X marks a reconnection site. The legs of large loops expanding into the heliosphere reconnect with adjacent open field lines. Crooker *et al.* [2004b] suggest that the expanding loops are at the quiet end of a spectrum of large-scale transient outflows, with coronal mass ejections (CMEs) at the active end. This interpretation is supported by the observation of coronal inflows and collapsing loops at locations where the HCS is inclined to the solar rotation direction [Sheeley and Wang, 2001], taken to be signatures of magnetic reconnection. The association of inverted HMF with the HCS suggests the solar origin of the expanding loops can be bipolar helmet streamers which surround the coronal source-surface neutral line and separate magnetic flux from coronal holes of opposite magnetic polarity, e.g., the two polar coronal holes at solar minimum. This paper also

considers unipolar streamers, called “pseudostreamers,” as an additional source.

[6] Pseudostreamers are very similar to bipolar streamers in coronagraph observations. They are also formed at the boundary between coronal magnetic flux from two different coronal holes, but unlike bipolar streamers, the flux at both foot points is of the same polarity, and thus, they do not contain current sheets [e.g., Eselevich, 1998; Eselevich *et al.*, 1999; Zhao and Webb, 2003; Wang *et al.*, 2007]. There has recently been much interest in pseudostreamers as a possible source of the slow solar wind [Crooker *et al.*, 2012; Riley and Luhmann, 2012], either through the expansion of coronal magnetic flux tubes [Wang *et al.*, 2012], or through the intermittent release of plasma by the opening of coronal loops via magnetic reconnection [Antiochos *et al.*, 2011]. Crooker *et al.* [2012] demonstrate that pseudostreamers occur in belts which are topologically connected to the bipolar streamer belt, thus forming a network of slow solar wind sources.

[7] In this study, we investigate the properties and solar origin of inverted heliospheric magnetic flux during the period 1998 to 2011, for which almost continuous HMF and STE data are available from the Advanced Composition Explorer (ACE) spacecraft. In particular, comparisons are made with the locations of bipolar and pseudostreamers estimated using the potential-field source-surface (PFSS) model of the corona.

2. Detection of HMF Inversions

[8] The orientation of the HMF in near-Earth space is determined from 64 s magnetic field observations made by the ACE spacecraft [Smith *et al.*, 1998]. Electron pitch-angle distributions (PADs) from the ACE Solar Wind Electron, Proton, and Alpha Monitor (SWEPAM)-E instrument [McComas *et al.*, 1998] are used to define the strahl direction at 64 s resolution. The 272 eV energy channel is used, as it

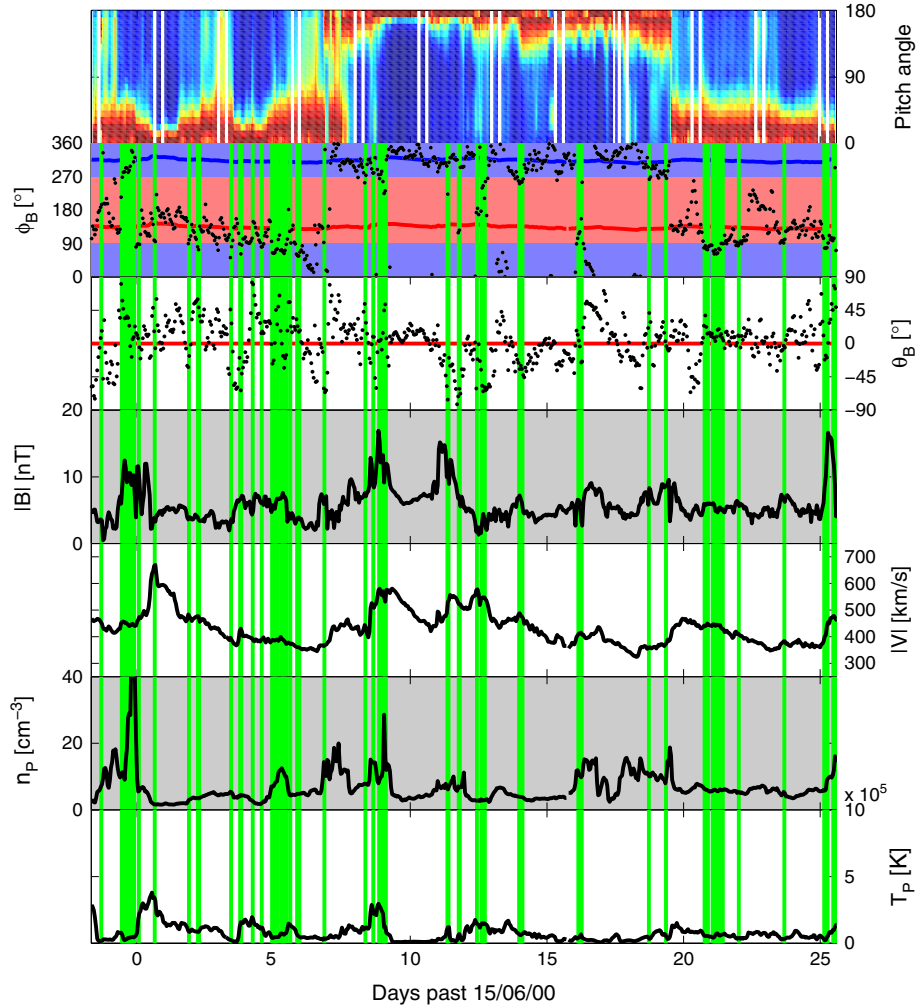


Figure 2. The observed near-Earth solar wind during Carrington rotation 1964 (13 June 2000 to 10 July 2000), which contains the greatest density of inverted HMF. Panels from top to bottom show the following: (a) Normalized 272 eV electron pitch-angle distributions, (b) in- and (c) out-of-ecliptic magnetic field angles in GSE coordinates, (d) magnetic field intensity, (e) solar wind speed, (f) density, and (g) temperature. The red and blue shaded regions in the second panel show sunward and antisunward directions, respectively, while the red and blue colored lines show the outward and inward ideal Parker spiral directions. Green vertical lines show the inverted flux regions.

is well within the suprathermal range, showing little contribution from the core electron population, but still providing high count rates [e.g., *Anderson et al.*, 2012]. The SWEPAM PAD data are available from January 1998 to August 2011, which determines the interval used in this study.

[9] The first step is to determine the suprathermal electron strahl direction. A number of methods exist to characterize the properties of the strahl from the electron pitch-angle distributions [e.g., *Hammond et al.*, 1996; *Anderson et al.*, 2012]. These generally involve fitting the observed PAD with an assumed functional form in order to determine strahl intensity, pitch-angle width, etc. For this study, the properties of the strahl are not required; only information about whether parallel and/or antiparallel strahls is present. Thus, we can use a much simpler and less computationally expensive method to process the PAD data. For each 64 s PAD, we compute the “background” flux by taking the mean flux across the four pitch-angle (PA) bins centered at 90° PA.

This is compared to the flux parallel and antiparallel to the magnetic field, defined as the mean flux over the four PA bins closest to 0 and 180° PA, respectively. If the parallel (antiparallel) flux exceeds the background flux by at least 100%, then the parallel (antiparallel) strahl is deemed to be present. If neither strahl meets the criteria, then the interval is categorized as undetermined. Conversely, if both parallel and antiparallel strahls are present, then the interval is classified as counterstreaming. We note, however, that this method is unable to discriminate between closed HMF and 90° pitch-angle depletions owing to mirroring from large-scale, downstream structures [*Gosling et al.*, 2001], so closed flux occurrence is likely overestimated. Furthermore, while counterstreaming electron intervals are separated out from inverted and uninverted flux, no attempt is made to explicitly exclude ICMEs. Indeed, if ICMEs contain “open” inverted field lines, then they must result from reconnection in the corona in the same way as ambient solar wind

intervals [Owens and Crooker, 2006, 2007]. By including all solar wind data in the study, no assumptions are made about the source and processes involved in the creation of inverted HMF.

[10] The 64 s magnetic field data is then used to determine whether the magnetic field is sunward- or antisunward-directed. In order to remove times in which the HMF lies approximately perpendicular to the heliocentric radial direction, times in which the radial magnetic field component has magnitude below 2 nT are classified as undetermined orientation. While not used to compute HMF topology, we additionally produce a 64 s time series of magnetic sector polarity, for comparison with model sector structure (section 4). This is determined by comparison to the ideal inward and outward Parker spiral directions using the observed solar wind speed.

[11] HMF topology is then determined by combining the magnetic field and electron data. Uninverted intervals are defined as those in which the magnetic field points antisunward and the strahl is parallel to it, or the magnetic field points sunward and the strahl is antiparallel to it. Conversely, inverted intervals contain either antisunward field with antiparallel strahl or sunward field with parallel strahl. In this manner, we create a time series of HMF topology at 64 s resolution. It is thus very sensitive to small-scale fluctuations such as waves and turbulence. In order to determine the larger-scale topology, the time series is split into 1 h intervals, each containing approximately 56 data points. In each 1 h interval, we determine whether the dominant topology is uninverted, inverted, counterstreaming, or undetermined. By first computing HMF topology at high time resolution, we avoid a number of potential misinterpretations. For example, a 1 h interval which contains a sector boundary with different strength strahls on either side could be misidentified as an inverted flux region if computed directly from hourly data.

[12] By choosing to define inverted HMF relative to the radial direction, as described above, we are explicitly identifying magnetic structures which currently thread a heliocentric sphere at 1 AU but no longer thread the coronal source surface. For completeness, we note that when we instead define inverted HMF relative to the ideal Parker spiral direction, as in Kahler *et al.* [1998], the results outlined in this study are essentially unchanged.

[13] As an example of topology determination, Figure 2 shows 1 h data for Carrington rotation (CR) 1964, which covers the period 13 June 2000 to 10 July 2000, and contains the highest density of inverted flux intervals in the entire 1998–2011 period. The top panel shows a normalized pitch angle—time spectrogram of the 272 eV electrons, with red indicating maximum flux and blue minimum. The spectrogram reveals that the strahl electrons were close to 0° pitch angle at the start and end of the CR but were consistently near 180° throughout the middle of the CR. Magnetic field data are shown in the second, third, and fourth panels. The second panel shows ϕ_B , the in-ecliptic magnetic field angle in Geocentric Solar Ecliptic (GSE) coordinates. Sunward and antisunward directions are shaded red and blue, respectively. For reference, outward and inward ideal Parker spiral angles computed from the observed solar wind speed are shown as solid red and blue lines, respectively. Observed magnetic field angles are plotted as black crosses. On the

Table 1. The Number of 1 h Observation Periods of Different HMF Populations Obtained Using the Magnetic Field and Suprathermal Electron Selection Criteria

		# 1 h Intervals	% of Available Data
Magnetometer data	Sunward HMF	53,714	44.9%
	Antisunward HMF	56,584	47.3%
	Undetermined	9,366	7.83%
Suprathermal electron data	Inward sector	60,252	50.4%
	Outward sector	59,041	49.3%
	Undetermined	371	0.31%
Suprathermal electron data	Parallel strahl	37,961	31.7%
	Antiparallel strahl	37,774	31.6%
	Counterstreaming	17,023	14.2%
	Undetermined	26,906	22.5%
Combined data sets	Uninverted	57,345	48.0%
	Inverted	6,608	5.53%
	Counterstreaming	19,388	16.2%
	Undetermined	36,139	30.2%

large scale, CR1964 shows a clear two-sector structure, with HCS crossings around 22 June 2000 and 4 July 2000, in rough agreement with the electron data. The third panel shows θ_B , the out-of-ecliptic magnetic field angle, in GSE coordinates, while the fourth panel shows magnetic field magnitude. Fifth to seventh panels show proton speed, density, and temperature, respectively. Vertical green lines mark inverted flux regions. They range from gradual rotations of the magnetic field direction away from the Parker spiral to inverted status, such as days 5–6 and 21–22, to Parker spiral-aligned fields with sunward strahls, such as days 0 and 16. We note that our strict criteria for selecting inverted flux intervals eliminates some cases near sector boundaries, for example, on day 7, owing to isotropization of the electron distribution near the heliospheric current sheet.

[14] Applying the selection criteria to the entire 1998 to 2011 interval results in the statistics reported in Table 1. There are 57,345 1 h intervals (48.0% of the total data set) with predominantly a single antisunward strahl, meaning the HMF is “uninverted,” as expected by the standard Parker model. There are 19,388 1 h intervals (16.2%) which exhibit both 0° and 180° strahls and so are classified as counterstreaming electrons (CSEs), while there are 6608 intervals (5.53%) exhibit sunward strahl resulting from inverted HMF. This leaves 36,139 intervals (30.2%) classified as undetermined, predominantly the result of not being able to identify a sufficiently strong strahl with our simple criteria. If the undetermined intervals are assumed to exhibit no systematic bias in any one HMF distribution, then the occurrence rates of uninverted/counterstreaming/inverted HMF are 68.8%/23.3%/7.92%. We note that Kahler *et al.* [1998] analyzed ISEE 3 observations from 1978 to 1982 and found HMF inversions comprised 6–8% of the data, consistent with our findings and suggesting that there has not been a significant change in the inverted HMF occurrence rate between the periods considered.

[15] Figure 3 shows time variations of three Carrington-rotation averages of occurrence rates of the different HMF populations over the entire period of the study. Its primary purpose is to demonstrate that the inverted HMF intervals are not confined solely to one portion of the

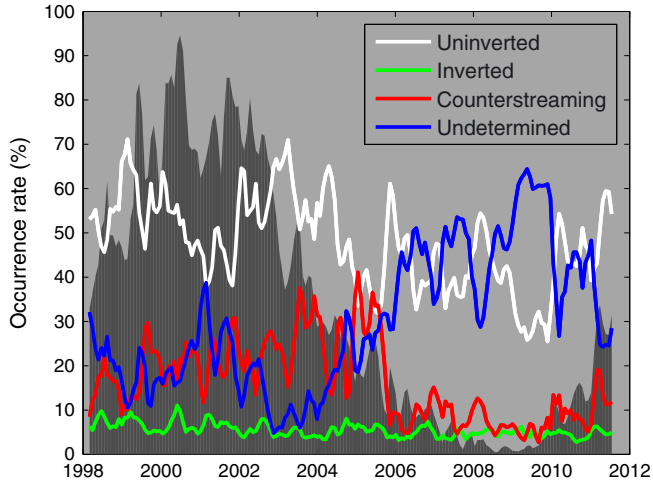


Figure 3. Three Carrington rotation averages of the occurrence rates of various HMF topologies as a function of time. Sunspot number, scaled to fit the axis, is shown as the dark-shaded region. Although some changes in the various HMF populations are likely to be due to changes in the electron detector, what this figure makes clear is that inverted flux is detected throughout the solar cycle.

solar cycle. The average detection rate of inverted HMF is approximately constant throughout the period of this study. Although both long-term drift and rapid changes to the detector gains on the SWEPAM-E instrument (details of which can be found at the ACE Science Center, <http://www.srl.caltech.edu/ACE/ASC/>) preclude unambiguous determinations of solar cycle variations, our analysis

should be somewhat robust to instrumental gain changes because we consider only strahl strength relative to the background level. The sharpness of the drop in CSE around 2005 may be an instrumental effect to some extent, but it is coincident with an observed drop in the CME/ICME rate [Owens *et al.*, 2008b; Richardson and Cane, 2012]. Similarly, the increase in undetermined intervals during solar minimum could be due to instrumental effects or to lengthy periods of skimming close to the heliospheric current sheet, where the electron distributions tend toward isotropy.

3. Properties of HMF Inversions

[16] Figure 4 shows the probability distribution functions (PDFs) of 1 h solar wind parameters. The total solar wind over the 1998–2011 interval is shown as a dark-shaded region. The various HMF populations determined in section 2 are shown as colored lines. The solar wind properties of uninverted HMF, shown in white, are similar to those seen over complete solar cycles [see also Hapgood *et al.*, 1991], though we note that uninverted flux has a higher average proton temperature than the solar wind in general. This is predominantly due to the undetermined component of the HMF having lower than average proton temperature, characteristic of the slow wind, where electron distributions tend to be more isotropic. Counterstreaming intervals are generally associated with stronger magnetic fields, reduced densities, and high solar wind speeds. The bimodal nature of the temperature PDF for CSEs suggests both hot and cold populations are present. Consequently, a significant fraction of the CSE intervals have low proton beta values. These signatures reflect the strong association of CSEs with closed

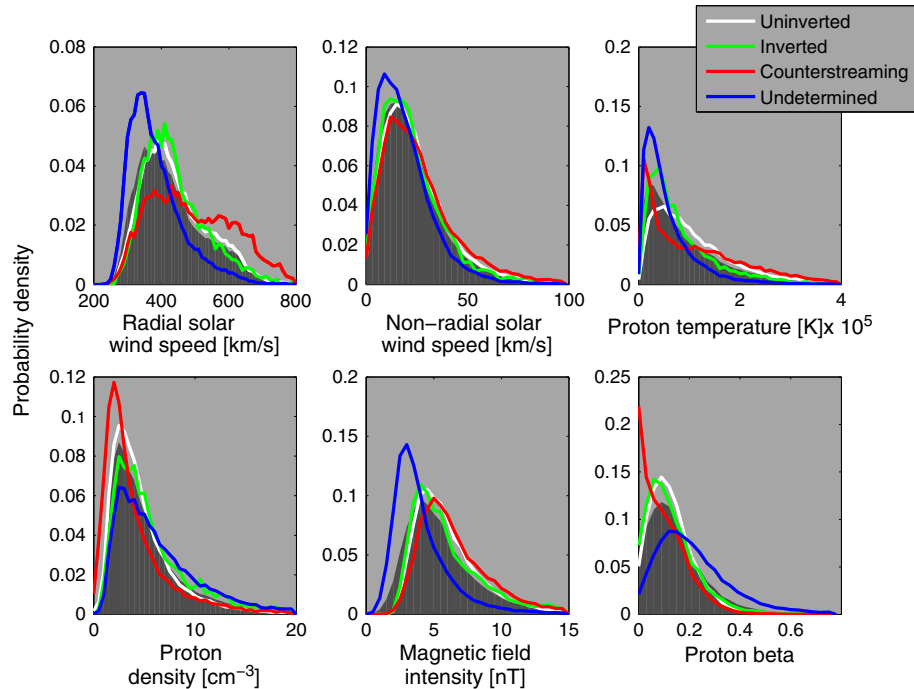


Figure 4. Probability distribution functions for various near-Earth solar wind populations. The grey-shaded region shows all solar wind in the interval 1998–2011. Colored lines show subsets of these data: White, green, red, and blue lines show uninverted, inverted, counterstreaming, and undetermined HMF intervals, respectively.

magnetic fields within ICMEs [Wimmer-Schweingruber *et al.*, 2006]. The extended tail of the nonradial flow speed PDF for CSE intervals is also in agreement with a strong ICME association [Gosling *et al.*, 1987; Owens and Cargill, 2004]. Inverted HMF exhibits solar wind characteristics similar to those in uninverted HMF. In particular, similar nonradial solar wind speeds suggest that draping of HMF in front of fast ICMEs [McComas *et al.*, 1988] is not a major source of HMF inversion. Inverted HMF is associated with lower average temperatures than uninverted HMF, along with slightly lower average magnetic fields and slightly higher average densities, suggestive of heliospheric plasma sheets [Crooker *et al.*, 2004a]. However, these properties do not seem to be present within the same intervals, since there is little difference in the proton beta for inverted and uninverted HMF. Undetermined HMF is generally low speed, high beta plasma, and consistent with greater scattering of the strahl.

4. Association With Bipolar and Pseudostreamers

[17] The in situ data shown in Figure 2 suggest that inverted flux intervals are not confined to regions close to the large-scale polarity inversions seen as a heliospheric current sheet crossing. From in situ observations alone, however, we cannot rule out the possibility that the HCS is slightly above/below the ecliptic and hence still associated with the inverted HMF, even though it is not intercepted by the observing spacecraft. Thus, to aid in the interpretation of these data, we use a potential-field source-surface (PFSS) model of the corona [Schatten *et al.*, 1969] based on Wilcox Solar Observatory (WSO) magnetograms to identify the locations of the HCS and, hence, bipolar streamers as well as pseudostreamers.

4.1. Case Studies

[18] CR1990, spanning approximately 23 May 2003 to 19 June 2003, is the period which gives the best match between the observed magnetic sector structure and that derived from the PFSS model, discussed further below. Thus, it is assumed that the PFSS model provides a good reconstruction of the global coronal magnetic field throughout CR1990. The top plot of Figure 5 shows a latitude-longitude map of the PFSS solution for Carrington rotation 1990. The pink and light grey regions show, respectively, outward and inward polarity coronal holes, i.e., the photospheric foot points of magnetic field lines which reach the source surface at 2.5 solar radii. Red (white) lines show the magnetic connection between the photosphere and the ecliptic plane's intersection with the source surface, for outward (inward) polarity magnetic fields. They were obtained by tracing magnetic fields through the PFSS solution to the corona. Overlaid on the ecliptic plane is the observed magnetic polarity in near-Earth space, ballistically mapped back to the source surface using the observed solar wind speed, with red/white dots indicating outward/inward Parker spiral HMF, as determined in section 2. For this particular Carrington rotation, there is excellent agreement between the magnetic polarity predicted by the PFSS model and that observed near-Earth. Green crosses show the coronal source-surface locations of observed HMF inversions at the heliographic latitude of Earth.

[19] The two intervals of inverted HMF at Carrington longitude of 310° coincides with a change in magnetic connection from the inward polarity coronal hole in the northern solar hemisphere to the outward polarity coronal hole in the southern hemisphere. Thus, these inverted HMF intervals are associated with the HCS and a bipolar streamer. Note that inverted HMF is not always present at the HCS, as demonstrated by the absence of inversions around 110° Carrington longitude. The remaining HMF inversions are also associated with a change in magnetic connectivity, with the photospheric foot points along Earth orbit shifting between different coronal holes, but without an associated change in foot point polarity, indicative of pseudostreamers. These HMF inversions are thus associated with pseudostreamers rather than bipolar streamers.

[20] The middle panel of Figure 5 illustrates a new method for quantifying changing photospheric connectivity. We first define a parameter dS , the distance between photospheric foot points of neighboring points on the source surface. In practice, the magnitude of dS will depend on the spatial resolution at which field lines are traced, making units somewhat arbitrary. In this study, we calculate dS by moving along the ecliptic plane in 1° steps. When adjacent points on the source surface map to the same coronal hole, dS will be small, for example, as seen between 0° and 60° Carrington longitude for CR1990. When neighboring source-surface points map to different coronal holes, however, such as the HCS crossing at 310° Carrington longitude, dS will be very large. The middle panel of Figure 5 shows $\log_e(dS)$ as a function of Carrington longitude along the ecliptic plane. Vertical yellow lines mark HCS crossings, where $\log_e(dS)$ spikes correspond to bipolar streamers. The dashed horizontal line at $\log_e(dS) = 3$ marks the threshold selected to define a streamer. It is the value which $\log_e(dS)$ reaches or exceeds at all HCS crossings in the 1998 to 2011 period and corresponds to source surface points with a 1° separation having a photospheric foot point separation of $\geq 5^\circ$. It thus selects all bipolar streamers and appears to select most significant pseudostreamers while suppressing smaller structures. Blue vertical lines mark $\log_e(dS)$ spikes without polarity reversals, our definition of a pseudostreamer. The 17 1 h intervals of inverted HMF not associated with the HCS in CR1990 all map close to the longitudes of pseudostreamers.

[21] The bottom panel of Figure 5 is a contour plot of dS at all latitudes. It demonstrates in another way the finding reported by [Crooker *et al.*, 2012] that pseudostreamer belts do not exist in isolation but connect to the bipolar streamer belt to form a network of slow solar wind sources that expands to cover the source surface during solar maximum. As is the case for bipolar streamers, HMF inversions are not associated with all pseudostreamers; however, Figure 5 demonstrates that streamer-associated inverted HMF is likely to be common at all latitudes near solar maximum.

[22] We use a maximum longitudinal separation of 13° to associate streamers with inverted HMF intervals (discussed below, as part of the statistical analysis). For CR1990, this means all 19 HMF inversions are associated with streamers; two map to bipolar streamers, 17 to pseudostreamers. In order to assess the significance of this result, it is necessary

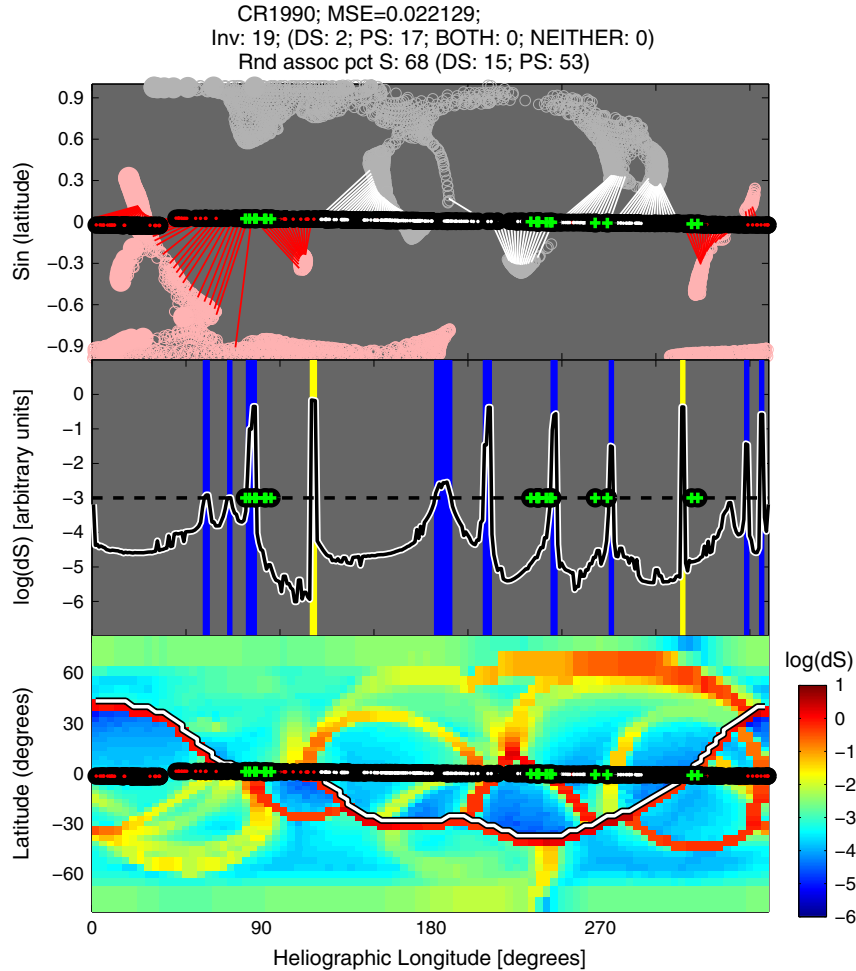


Figure 5. (top) A latitude-longitude map of the PFSS solution for Carrington rotation 1990. Pink/dark grey regions are the PFSS inward/outward coronal holes, with red/white lines showing the connection between the Earth's orbit across the source surface and photosphere. Overlaid on the black strip are red/white dots showing the observed outward/inward sectors mapped to the source surface. Green crosses are inverted flux intervals. (middle) dS , photospheric foot point separation for adjacent points on the source surface, along the ecliptic plane (shown on a \log_e scale). This parameter serves as a means of identifying coronal streamers: Bipolar (pseudo) streamers are shown as vertical yellow (blue) lines. (bottom) Contour plot of dS over all latitudes of the source surface. The HCS is the white curve.

to compare it with the probability of the same associations occurring purely by chance. For CR1990, 68% of the ecliptic path is within 13° of a streamer. Thus, the probability of 19 independent solar wind intervals being randomly associated with streamers is $(0.68)^{19} = 0.0007$.

[23] Figure 6 shows a second example, CR2011 (approximately 17 December 2003 to 13 January 2004), the second most accurate PFSS reconstruction. The streamer network is slightly less dense and covers less area, consistent with contraction as the solar cycle progresses [Crooker *et al.*, 2012]. Applying the longitudinal tolerance of 13° , we find that streamers cover 56% of the ecliptic path. There are 27 inverted HMF intervals in this period; 6 map to bipolar streamers, 15 map to pseudostreamers, and 6 are not associated with any streamers. We note that the inverted HMF intervals around 100° and 290° Carrington longitude are associated with rises in dS , but they are not sufficient to qualify as streamers.

4.2. Statistical Analysis

[24] In order to systematically analyze the entire 1998–2011 interval, we must include only CRs in which the PFSS model is valid and define strict thresholds for association between inverted HMF and streamers. We begin by including only Carrington rotations in which the PFSS model provides a reasonable representation of the observed magnetic structure of the corona and solar wind. By assigning +1 (–1) to outward (inward) Parker spiral polarity and ignoring undetermined, counterstreaming, and inverted intervals, we compute the mean-square error (MSE) between the PFSS and observed sector structure mapped to the source surface. Thus, MSE is a combination of errors in the PFSS solution and errors in the simple ballistic mapping of near-Earth solar wind to the coronal source surface. CR1990 has an MSE of 0.02, while CR2011 has 0.05. For inclusion in this study, we set a limit of $\text{MSE} < 0.3$ for each Carrington rotation, equivalent to correct magnetic field polarity predictions for at least

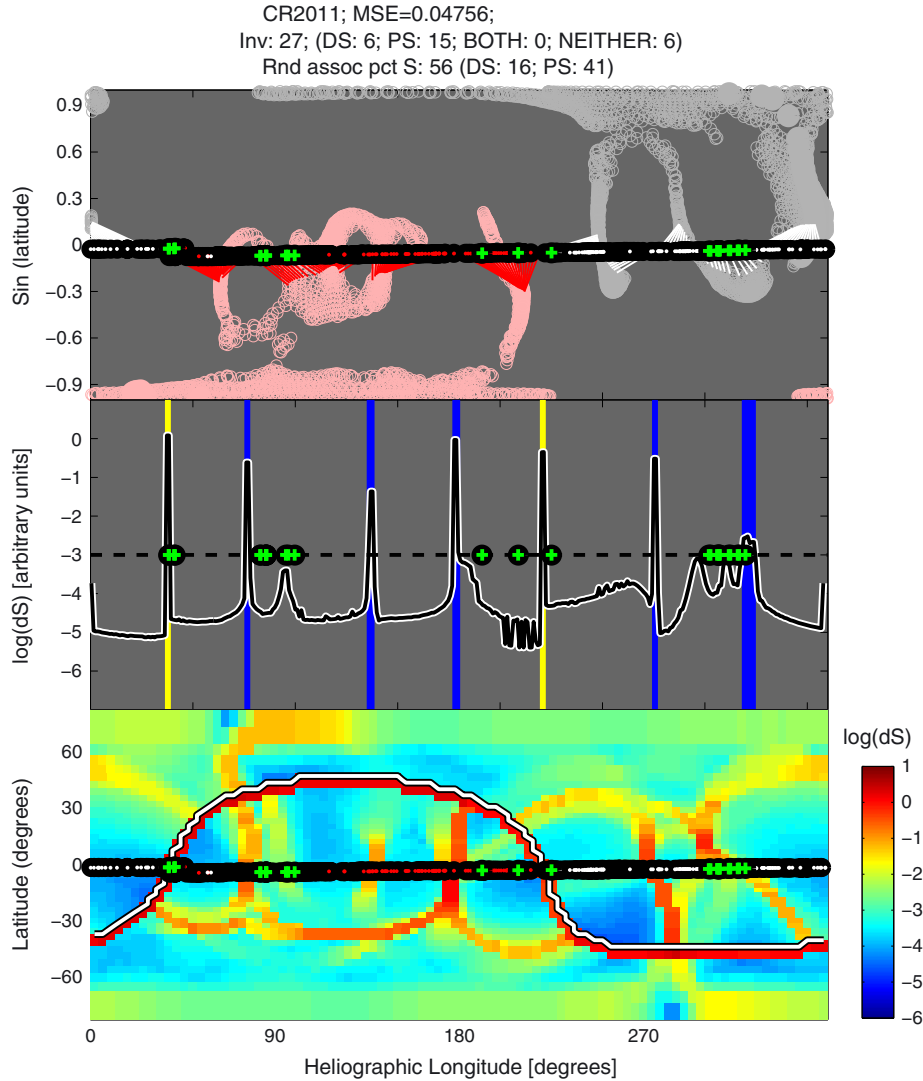


Figure 6. Parameters for Carrington rotation 2011, in the same format as Figure 5.

95% of the hourly intervals. This leaves 63 Carrington rotations, approximately 35% of the total data set, with a slight bias toward the declining phase of the solar cycle. These CRs contain 2263 intervals of inverted HMF, an occurrence rate of 5.5%. Thus, these 63 Carrington rotations appear to be representative of the whole 1998–2011 interval. For the selected Carrington rotations, the average error between the PFSS and observed HCS longitude is 13° . We set this value as the longitudinal tolerance for association between inverted HMF and streamers.

[25] Application of the streamer detection and association criteria to all 63 suitable Carrington rotations results in 1312 of the 2263 inverted HMF intervals (58%) associated with streamers. This number should be treated as a lower limit in view of streamer associations missed owing to electron distributions approaching isotropy near sector boundaries. On average, 52% of the ecliptic plane is within 13° of a streamer; thus, a random solar wind interval has a 52% chance of being associated with a streamer by our scheme. A Monte Carlo analysis of 1310 random solar wind intervals assuming a 52% chance of streamer association suggests the observed association between inverted

HMF and streamers is significant at the 99.9% level. Similarly, looking at the inverse result, only 42% of the inverted HMF intervals have no streamer association, while the probability of a random solar wind interval not being associated with a streamer is 48%. This difference is again 99.9% significant. Of the 1312 streamer-associated inverted HMF intervals, 949 (504) map to pseudostreamers (bipolar streamers), while 39% (21%) of ecliptic longitudes are covered by pseudostreamers (bipolar streamers). Note that the association scheme allows a single inverted HMF interval to map to both a bipolar and pseudostreamer if they are located close in longitude. Table 2 summarizes these results.

[26] In general, there are insufficient inverted HMF events to detect significant differences in the probability distribution functions of solar wind properties of bipolar- and pseudostreamer-associated inversions. Probability distributions of density, however (not shown), suggest that HMF inversions from bipolar streamers contain denser solar wind than inverted HMF from pseudostreamers, consistent with general properties of pseudostreamer-associated solar wind [Wang *et al.*, 2012].

Table 2. Solar Origins of the Inverted HMF Intervals^a

	Total	Any Streamer	Pseudo (PS)	Bipolar (DS)	Both PS and DS	No Streamer Association
Inverted HMF (% of total)	2263 -	1310 (57.9%)	949 (41.9%)	504 (22.3%)	143 (6.3%)	953 (42.1%)
Random interval	-	52.4%	39.0%	20.5%	5.1%	47.6%

^aAlso shown is the probability that a random solar wind interval would be associated with the given type of streamer, i.e., the percentage of ecliptic longitudes which are associated with different coronal structures.

5. Conclusions and Discussion

[27] The polarity of the photospheric foot point of heliospheric magnetic flux (HMF) can be independently estimated from both the local HMF orientation, as measured using in situ magnetometer observations, and the direction of the suprathermal electron beam, or “strahl.” For the bulk of the solar wind, these two methods show agreement. There are intervals, however, in which the strahl is directed toward the Sun, implying that the magnetic field line is inverted, or folded back on itself. This is an expected signature of near-Sun magnetic reconnection by which the Sun can open previously closed heliospheric loops [Owens *et al.*, 2011; Owens and Lockwood, 2012]. Using an automated data analysis method, we find inverted flux in approximately 5.5% of the solar wind data between 1998 and 2011, though this is likely an underestimate due to strict selection criteria. We do not find a strong solar cycle variation in the occurrence rate of inverted HMF, but this finding is confined to the ecliptic plane and may be complicated by changing instrument characteristics. Inverted HMF is associated with dense, slow, cool solar wind, with lower than average magnetic field intensity. In order to determine the solar origin of these structures, we used a potential-field source-surface model to infer the global structure of the coronal magnetic field and a new automated detection method for bipolar and pseudostreamers. Of the 2263 1 h inverted HMF intervals identified in the solar wind and mapped back to the coronal source surface, 1310 (58%) are associated with streamers. Given that the probability of a solar wind interval being associated with a streamer by chance is 52%, the association between inverted HMF and streamers is significant at the 99.9% level. Of the 1310 streamer-associated inverted HMF intervals, 949 (504) map to pseudostreamers (bipolar streamers). This ratio is in reasonable agreement with the occurrence rates of pseudostreamers and bipolar streamers in the ecliptic plane, 39% and 20%, respectively, suggesting similar inverted flux production rates.

[28] Conversely, 42% of the 1 h inverted HMF intervals are not associated with streamers. There are two possible explanations. First, that these intervals were produced at streamers, but our analysis is not able to make the association, either because of inaccuracies in the PFSS reconstruction of the corona, the criteria used to define streamers or the ballistic propagation from 1 AU to the source surface. Second, that these inverted HMF intervals are not the result of streamers, instead being produced by some other process like draping of HMF at the front of ICMEs [McComas *et al.*, 1988] and reconnection in the solar wind [Gosling *et al.*, 2007] or solar wind stream shear [Lockwood *et al.*, 2009].

Draping, however, has already been discussed as unlikely owing to no increase in nonradial speeds, and the strong association of inverted HMF with pseudostreamers suggests magnetic reconnection in the heliosphere [Gosling *et al.*, 2005; Phan *et al.*, 2006] is not the predominant source of inverted HMF. While heliospheric reconnection is possible for low magnetic shear angles [e.g., Gosling *et al.*, 2007], the unipolar HMF from pseudostreamers would not provide any more preferential conditions for reconnection than other locations in the solar wind.

[29] If we assume that inverted HMF is primarily a signature of reconnection in the corona [e.g., Titov *et al.*, 2011], then our results suggest that the rate of reconnection is similar within bipolar and pseudostreamers. This seems reasonable in view of their magnetic structure. For the bipolar streamer case, a three-dimensional magnetic configuration for interchange reconnection that can create the inversion is illustrated in Figure 1e and has already been discussed in section 1. For the pseudostreamer case, an appropriate magnetic configuration can be drawn in just two dimensions, as illustrated in Figure 7. Closed loops within one of the two arcades that form pseudostreamers are shown to rise as a result of photospheric flux emergence but could equally be the result of loop foot point shearing, etc. In the top panel, the rising loop undergoes interchange reconnection before it reaches the solar wind acceleration height and therefore does not result in the generation of inverted HMF. This configuration is common from the solar perspective [e.g., Wang *et al.*, 2007; Crooker *et al.*, 2012]. In contrast, from the heliospheric perspective, the rising loops are dragged out by the solar wind before interchange reconnection takes place, which does generate inverted HMF, as illustrated in the bottom panels. Thus, pseudostreamer loop expansion and opening via interchange reconnection would transport preexisting open solar flux in much the same way as the CME-driven transport proposed by Owens *et al.* [2007]. Indeed, as proposed by Crooker *et al.* [2004b] for loops expanding from the helmet arcade in the case of bipolar streamers, loops that create inversions from pseudostreamers can also be considered as the quiet end of a spectrum of loops, where the active end is CMEs. This analogy holds because pseudostreamers are well-documented sources of CMEs [Fainshtein, 1997; Eselevich *et al.*, 1999; Zhao and Webb, 2003; Liu and Hayashi, 2006].

[30] In addition, similar levels of association between inverted HMF with bipolar and pseudostreamers, despite the differing magnetic topologies, suggest that the reconnection rate is externally controlled. One possibility is the stress between the differential rotation of the photosphere and the

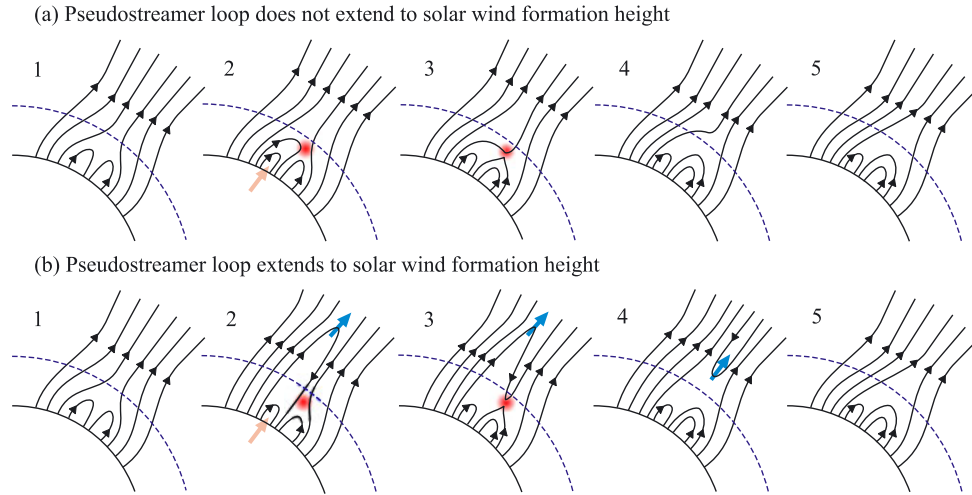


Figure 7. A sketch of time evolution of interchange reconnection within a pseudostreamer. In the top panel, a closed loop rises due to photospheric flux emergence (red arrow) but does not reach the solar wind acceleration height (blue-dashed line) before it undergoes reconnection with an open magnetic field line. This creates an Alfvén wave on the open magnetic field line which propagates out into the heliosphere but does not create inverted HMF. The bottom panels show a loop which is dragged out by the solar wind (blue arrow) before interchange reconnection occurs. It does result in the creation of inverted HMF.

rigid corotation of the corona [Nash *et al.*, 1988; Wang and Sheeley, 2004] and the consequent circulation of open solar flux [Fisk *et al.*, 1999; Fisk and Schwadron, 2001]. We note that inverted HMF is the expected heliospheric signature of large coronal loop opening, one of the proposed mechanisms for slow solar wind formation [e.g., Fisk, 2003]. Thus, our results provide support for the idea of pseudostreamers being a source of slow solar wind through intermittent release from previously closed coronal loops [Antiochos *et al.*, 2011], though the effect of magnetic flux tube expansion [Wang *et al.*, 2012] may still be important.

[31] Inverted HMF has direct implications for in situ spacecraft estimates of the total magnetic flux threading the solar source surface, often referred to as the unsigned open solar flux (OSF) [e.g., Owens *et al.*, 2008a]. Figures 1c and 1d clearly illustrate the issue: Inverted HMF provides magnetic flux which threads the heliocentric sphere at 1 AU but does not map back to the source surface, resulting in an overestimate in OSF from in situ observations. As inverted HMF intervals can be Parker spiral aligned (e.g., day 0 in Figure 2), decomposing the HMF along the Parker spiral direction, which can successfully remove the effects of waves and turbulence [Erdős and Balogh, 2012], may not address this particular issue. Both the occurrence rate and magnetic field strength associated with inverted HMF are small, suggesting this may not have a large effect on OSF estimates. Even if inverted HMF has an average magnetic flux density as high as the rest of the solar wind, the decrease in the unsigned OSF would only be $2 \times 5\% = 10\%$. The factor 2 arises as follows: If inverted HMF intervals contain ϕ_I of magnetic flux, then the unsigned OSF will be overestimated by $2\phi_I$, since both the inverted and “return” flux thread the heliocentric surface but not the coronal source surface. We note that, in general, inverted HMF is clustered in intervals less than a day long, though this may be partly due

to the strict criteria used and the time interval considered [cf. Crooker *et al.*, 2004b]. Thus, taking 1 day averages of the radial magnetic field for the purposes of estimating OSF may indirectly negate the effect of inverted HMF [cf. Wang and Sheeley, 1995], though it does not directly address the issue of physical origin (see also Lockwood *et al.* [2009] for discussion of correction of 1 AU measurements to the coronal source surface).

[32] In summary, we have developed a new method for identifying bipolar streamers and pseudostreamers in PFSS synoptic maps. The results confirm that together, these structures form a network of slow solar wind sources which expands over the source surface at solar maximum. Moreover, we have analyzed suprathermal electron data from the solar wind and find that, like bipolar streamers, pseudostreamers are sources of HMF inversions. These are understood to be signatures of coronal loops that expand into the heliosphere and subsequently become open through reconnection in the corona. Loop-opening is a key process in one of two competing models for the source of the slow wind.

[33] **Acknowledgments.** We are grateful to the ACE Science Center (ASC) for magnetic field and suprathermal electron data, and to T. Hoeksema of Stanford University for WSO magnetograms. Research for this paper was supported in part (NUC) by the U.S. National Science Foundation under grant AGS-0962645. This work was facilitated by the ISSI workshop 233, “Long-term reconstructions of solar and solar wind parameters” organized by L. Svalgaard, E. Cliver, J. Beer, and M. Lockwood. MO thanks Andre Balogh of Imperial College London for useful discussions. Philippa Browning thanks Christopher Owen and Ruth Skoug for their assistance in evaluating this paper.

References

Anderson, B. R., R. M. Skoug, J. T. Steinberg, and D. J. McComas (2012), Variability of the solar wind suprathermal electron strahl, *J. Geophys. Res.*, *117*, A04107, doi:10.1029/2011JA017269.

- Antiochos, S. K., V. Z. Mikić, S. Titov, R. Lionello, and J. A. Linker (2011), A model for the sources of the slow solar wind, *Astrophys. J.*, *731*, 112, doi:10.1088/0004-637X/731/2/112.
- Balogh, A., R. J. Forsyth, E. A. Lucek, T. S. Horbury, and E. J. Smith (1999), Heliospheric magnetic field polarity inversions at high heliographic latitudes, *Geophys. Res. Lett.*, *26*, 631–634, doi:10.1029/1999GL900061.
- Borovsky, J. E. (2010), On the variations of the solar wind magnetic field about the Parker spiral direction, *J. Geophys. Res.*, *115*, A09101, doi:10.1029/2009JA015040.
- Crooker, N. U., M. E. Burton, G. L. Siscoe, S. W. Kahler, J. T. Gosling, and E. J. Smith (1996), Solar wind streamer belt structure, *J. Geophys. Res.*, *101*, 24,331–24,342, doi:10.1029/96JA02412.
- Crooker, N. U., J. T. Gosling, and S. W. Kahler (1998), Magnetic clouds at sector boundaries, *J. Geophys. Res.*, *103*, 301.
- Crooker, N. U., C.-L. Huang, S. M. Lamassa, D. E. Larson, S. W. Kahler, and S. H. E. (2004a), Heliospheric plasma sheets, *J. Geophys. Res.*, *109*, A03107, doi:10.1029/2003JA010170.
- Crooker, N. U., S. W. Kahler, D. E. Larson, and R. P. Lin (2004b), Large-scale magnetic field inversions at sector boundaries, *J. Geophys. Res.*, *109*, A03108, doi:10.1029/2003JA010278.
- Crooker, N. U., S. K. Antiochos, X. Zhao, and M. Neugebauer (2012), Global network of slow solar wind, *J. Geophys. Res.*, *117*, A04104, doi:10.1029/2011JA017236.
- Erdős, G., and A. Balogh (2012), Magnetic flux density measured in fast and slow solar wind streams, *Astrophys. J.*, *753*, 130, doi:10.1088/0004-637X/753/2/130.
- Eselevich, V. G. (1998), On the structure of coronal streamer belts, *J. Geophys. Res.*, *103*, 2021, doi:10.1029/97JA02365.
- Eselevich, V. G., V. G. Fainstein, and G. V. Rudenko (1999), Study of the structure of streamer belts and chains in the solar corona, *Sol. Phys.*, *188*, 277–297.
- Fainstein, V. G. (1997), An investigation of solar factors governing coronal mass ejection characteristics, *Sol. Phys.*, *174*, 413–435.
- Feldman, W. C., J. R. Asbridge, S. J. Bame, M. D. Montgomery, and S. P. Gary (1975), Solar wind electrons, *J. Geophys. Res.*, *80*, 4181–4196.
- Fisk, L. A. (2003), Acceleration of the solar wind as a result of the reconnection of open magnetic flux with coronal loops, *J. Geophys. Res.*, *108*, 1157, doi:10.1029/2002JA009284.
- Fisk, L. A., and N. A. Schwadron (2001), The behaviour of the open magnetic field of the Sun, *Astrophys. J.*, *560*, 425–438.
- Fisk, L. A., T. H. Zurbuchen, and N. A. Schwadron (1999), Coronal hole boundaries and their interaction with adjacent regions, *Space Sci. Rev.*, *87*, 43–54.
- Gosling, J. T., D. N. Baker, S. J. Bame, W. C. Feldman, and R. D. Zwickl (1987), Bidirectional solar wind electron heat flux events, *J. Geophys. Res.*, *92*, 8519–8535.
- Gosling, J. T., S. J. Bame, W. C. Feldman, D. J. McComas, J. L. Phillips, and B. E. Goldstein (1993), Counterstreaming suprathermal electron events upstream of corotating shocks in the solar wind beyond approximately 2 AU: Ulysses, *Geophys. Res. Lett.*, *20*, 2335–2338, doi:10.1029/93GL02489.
- Gosling, J. T., R. M. Skoug, and W. C. Feldman (2001), Solar wind electron halo depletions at 90-degree pitch angle, *Geophys. Res. Lett.*, *28*, 4155–4158, doi:10.1029/2001GL013758.
- Gosling, J. T., R. M. Skoug, D. J. McComas, and C. W. Smith (2005), Magnetic disconnection from the sun: Observations of a reconnection exhaust in the solar wind at the heliospheric current sheet, *Geophys. Res. Lett.*, *32*, L05105, doi:10.1029/2005GL022406.
- Gosling, J. T., S. Eriksson, D. J. McComas, T. D. Phan, and R. M. Skoug (2007), Multiple magnetic reconnection sites associated with a coronal mass ejection in the solar wind, *J. Geophys. Res.*, *112*, 8106–+, doi:10.1029/2007JA012418.
- Haggerty, D. K., E. C. Roelof, C. W. Smith, N. F. Ness, R. L. Tokar, and R. M. Skoug (2000), Interplanetary magnetic field connection to the L1 Lagrangian orbit during upstream energetic ion events, *J. Geophys. Res.*, *105*, 25,123–25,132, doi:10.1029/1999JA000346.
- Hammond, C. M., W. C. Feldman, D. J. McComas, J. L. Phillips, and R. J. Forsyth (1996), Variation of electron-strahl width in the high-speed solar wind: Ulysses observations, *Astron. Astrophys.*, *316*, 350–354.
- Hapgood, M. A., G. Bowe, M. Lockwood, D. M. Willis, and Y. Tuluay (1991), Variability of the interplanetary magnetic field at 1 AU over 24 years: 1963–1986, *Planet. Space Sci.*, *39*, 411–423, doi:10.1016/0032-0633(91)90003-S.
- Kahler, S., and R. P. Lin (1994), The determination of interplanetary magnetic field polarities around sector boundaries using E greater than 2 keV electrons, *Geophys. Res. Lett.*, *21*, 1575–1578, doi:10.1029/94GL01362.
- Kahler, S., N. U. Crooker, and J. T. Gosling (1998), Properties of interplanetary magnetic sector boundaries based on electron heat-flux flow directions, *J. Geophys. Res.*, *103*, 20,603–20,612, doi:10.1029/98JA01745.
- Kahler, S. W., and R. P. Lin (1995), An examination of directional discontinuities and magnetic polarity changes around interplanetary sector boundaries using E > 2 keV electrons, *Sol. Phys.*, *161*, 183–195, doi:10.1007/BF00732092.
- Kahler, S. W., N. U. Crooker, and J. T. Gosling (1996), The topology of intrasector reversals of the interplanetary magnetic field, *J. Geophys. Res.*, *101*, 24,373–24,382, doi:10.1029/96JA02232.
- Liu, Y., and K. Hayashi (2006), The 2003 October–November fast halo coronal mass ejections and the large-scale magnetic field structures, *Astrophys. J.*, *640*, 1135–1141, doi:10.1086/500290.
- Lockwood, M., M. Owens, and A. P. Rouillard (2009), Excess open solar magnetic flux from satellite data: 2. A survey of kinematic effects, *J. Geophys. Res.*, *114*, A11104, doi:10.1029/2009JA014450.
- McComas, D. J., J. T. Gosling, D. Winterhalter, and E. J. Smith (1988), Interplanetary magnetic field draping about fast coronal mass ejecta in the outer heliosphere, *J. Geophys. Res.*, *93*, 2519–2526, doi:10.1029/JA093iA04p02519.
- McComas, D. J., S. J. Bame, S. J. Barker, W. C. Feldman, J. L. Phillips, P. Riley, and J. W. Griffee (1998), Solar wind electron proton alpha monitor (SWEPAM) for the Advanced Composition Explorer, *Space Sci. Rev.*, *86*, 563.
- Nash, A. G., N. R. Sheeley Jr., and Y.-M. Wang (1988), Mechanisms for the rigid rotation of coronal holes, *Sol. Phys.*, *117*, 359–389.
- Owens, M. J., and P. J. Cargill (2004), Non-radial solar wind flows induced by the motion of interplanetary coronal mass ejections, *Ann. Geophys.*, *22*, 4397–4395.
- Owens, M. J., and N. U. Crooker (2006), Coronal mass ejections and magnetic flux buildup in the heliosphere, *J. Geophys. Res.*, *111*, A10104, doi:10.1029/2006JA011641.
- Owens, M. J., and N. U. Crooker (2007), Reconciling the electron counterstreaming and dropout occurrence rates with the heliospheric flux budget, *J. Geophys. Res.*, *112*, A06106, doi:10.1029/2006JA012159.
- Owens, M. J., and M. Lockwood (2012), Cyclic loss of open solar flux since 1868: The link to heliospheric current sheet tilt and implications for the Maunder Minimum, *J. Geophys. Res.*, *117*, A04102, doi:10.1029/2011JA017193.
- Owens, M. J., N. A. Schwadron, N. U. Crooker, W. J. Hughes, and H. E. Spence (2007), Role of coronal mass ejections in the heliospheric Hale cycle, *Geophys. Res. Lett.*, *34*, L06104, doi:10.1029/2006GL028795.
- Owens, M. J., C. N. Arge, N. U. Crooker, N. A. Schwadron, and T. S. Horbury (2008a), Estimating total heliospheric magnetic flux from single-point in situ measurements, *J. Geophys. Res.*, *113*, A12103, doi:10.1029/2008JA013677.
- Owens, M. J., N. U. Crooker, N. A. Schwadron, T. S. Horbury, S. Yashiro, H. Xie, C. St O. C., and N. Gopalswamy (2008b), Conservation of open solar magnetic flux and the floor in the heliospheric magnetic field, *Geophys. Res. Lett.*, *35*, L20108, doi:10.1029/2008GL035813.
- Owens, M. J., N. U. Crooker, and M. Lockwood (2011), How is open solar magnetic flux lost over the solar cycle? *J. Geophys. Res.*, *116*, A04111, doi:10.1029/2010JA016039.
- Phan, T. D., et al. (2006), A magnetic reconnection X-line extending more than 390 Earth radii in the solar wind, *Nature*, *439*, 175–178, doi:10.1038/nature04393.
- Richardson, I. G., and H. V. Cane (2012), Near-earth solar wind flows and related geomagnetic activity during more than four solar cycles (1963–2011), *J. Geophys. Res.*, *2* (26), A02, doi:10.1051/swsc/2012003.
- Riley, P., and J. G. Luhmann (2012), Interplanetary signatures of unipolar streamers and the origin of the slow solar wind, *Sol. Phys.*, *277*, 355–373, doi:10.1007/s11207-011-9909-0.
- Rosenbauer, H., et al. (1977), A survey on initial results of the HELIOS plasma experiment, *J. Geophys.-Z. Geophys.*, *42*, 561–580.
- Schatten, K. H., J. M. Wilcox, and N. F. Ness (1969), A model of interplanetary and coronal magnetic fields, *Sol. Phys.*, *9*, 442–455.
- Sheeley, N. R., Jr., and Y.-M. Wang (2001), Coronal inflows and sector magnetism, *Astrophys. J. Lett.*, *562*, L107–L110, doi:10.1086/338104.
- Smith, C. W., J. L'Heureux, N. F. Ness, M. H. Acuna, L. F. Burlaga, and J. Scheifele (1998), The ACE magnetic fields experiment, *Space Sci. Rev.*, *86*, 613.
- Steinberg, J. T., J. T. Gosling, R. M. Skoug, and R. C. Wiens (2005), Suprathermal electrons in high-speed streams from coronal holes: Counterstreaming on open field lines at 1 AU, *J. Geophys. Res.*, *110*, A06103, doi:10.1029/2005JA011027.
- Titov, V. S., Z. Mikić, J. A. Linker, R. Lionello, and S. K. Antiochos (2011), Magnetic topology of coronal hole linkages, *Astrophys. J.*, *731*, 111, doi:10.1088/0004-637X/731/2/111.

- Wang, Y., and N. R. Sheeley Jr. (2004), Footpoint switching and the evolution of coronal holes, *Astrophys. J.*, *612*, 1196–1205, doi:10.1086/422711.
- Wang, Y.-M., and N. R. Sheeley Jr. (1995), Solar, implications of Ulysses interplanetary field measurements, *Astrophys. J. Lett.*, *447*, L143–L146, doi:10.1086/309578.
- Wang, Y.-M., N. R. Sheeley Jr., and N. B. Rich (2007), Coronal pseudostreamers, *Astrophys. J.*, *658*, 1340–1348, doi:10.1086/511416.
- Wang, Y.-M., R. Grappin, E. Robbrecht, and N. R. Sheeley Jr. (2012), On the nature of the solar wind from coronal pseudostreamers, *Astrophys. J.*, *749*, 182, doi:10.1088/0004-637X/749/2/182.
- Wimmer-Schweingruber, R. F., et al. (2006), Understanding interplanetary coronal mass ejection signatures, *Space Sci. Rev.*, *123*, 177–216, doi:10.1007/s11214-006-9017-X.
- Zhao, X. P., and D. F. Webb (2003), Source regions and storm effectiveness of frontside full halo coronal mass ejections, *J. Geophys. Res.*, *108*, 1234, doi:10.1029/2002JA009606.